Oblique Random Forests for 3-D Vessel Detection Using Steerable Filters and Orthogonal Subspace Filtering
– Supplementary Material –

Matthias Schneider[1], Sven Hirsch[1], Gábor Székely[1], Bruno Weber[2], and Bjoern H. Menze[1]

[1] Computer Vision Laboratory, ETH Zurich, Switzerland
[2] Institute of Pharmacology and Toxicology, University of Zurich, Zurich, Switzerland

A Appendix

A.1 Steerability of Gaussian Derivatives

The steerability of Gaussian derivatives has been derived for the 2-D case in [3] and can readily be extended to 3-D [2]. Steerability refers to the property that the convolution of an image with a rotated version of the steerable filter template (SFT) can be expressed by a linear combination of the filter response of the image with the SFT without rotation:

$$I * G^{\sigma}_{m,a,b}(R\boldsymbol{x}) = \sum_{i=0}^{m}\sum_{j=0}^{i} \omega^{i,j}_{m,a,b} \underbrace{\left(I * G^{\sigma}_{m,i,j}\right)(\boldsymbol{x})}_{\boldsymbol{f}^{\sigma}_{\boldsymbol{m,i,j}}(I,\boldsymbol{x})} \quad , \tag{1}$$

where $R \in SO(3)$ denotes a 3-D rotation matrix:

$$R_{\theta,\phi} = \begin{pmatrix} \cos\theta\cos\phi & \cos\theta\sin\phi & \sin\theta \\ -\sin\phi & \cos\phi & 0 \\ -\sin\theta\cos\phi & -\sin\theta\sin\phi & \cos\theta \end{pmatrix} \quad . \tag{2}$$

The uniquely defined coefficients $\omega^{i,j}_{m,a,b}$ can be computed in closed form as:

$$\begin{aligned} w^{i,j}_{m,a,b} = \sum_{\boldsymbol{s}\in\mathcal{S}^{i,j}_{m,a,b}} & (-1)^{a-v_1-w_2}\binom{m-a}{u_1}\binom{a-b}{v_1}\binom{b}{w_1}\binom{u_1}{u_2}\binom{w_1}{w_2} \\ & (\cos\theta)^{m-a-u_2+w_2}(\cos\phi)^{m-a+b-u_1+v_1-w_1} \\ & (\sin\theta)^{b+u_2-w_2}(\sin\phi)^{a-b+u_1-v_1+w_1-u_2-w_2} \quad , \end{aligned} \tag{3}$$

where

$$\begin{aligned} \mathcal{S}^{i,j}_{m,a,b} = \{(u_1,v_1,w_1,u_2,w_2)^{\mathrm{T}} \in \mathbb{N}_0^5 \mid & u_1 \le m-a,\ v_1 \le a-b, \\ & w \le b,\ u_2 \le u_1,\ w_2 \le w_1, \\ & u_1+v_1+w_1 = i, u_2+w_2 = j\} \quad . \end{aligned} \tag{4}$$

Proof. Following [3], the Fourier transformation (FT) of the rotated filter templates as defined in Equations (1) and (2) can be computed by a rotation in the Fourier domain:

$$\begin{aligned}\mathcal{F}\left(G^{\sigma}_{m,a,b}(R_{\theta,\phi}\boldsymbol{x})\right) = (\ & i\omega_x\cos\theta\cos\phi + i\omega_y\cos\theta\sin\phi + i\omega_z\sin\theta)^{m-a} \\ & (-i\omega_x\sin\phi \quad + i\omega_y\cos\phi \quad + 0 \quad)^{a-b} \\ & (-i\omega_x\sin\theta\cos\phi + i\omega_y\sin\theta\sin\phi + i\omega_z\cos\theta)^{b}\cdot\hat{G}^{\sigma}(\boldsymbol{\omega}) \quad ,\end{aligned} \tag{5}$$

where $\hat{G}^{\sigma}(\boldsymbol{x}) = \mathcal{F}(G^{\sigma}(\boldsymbol{x}))$ denotes the transfer function of the Gaussian kernel. Repeatedly applying the binomial equation, this can be rewritten as:

$$\begin{aligned}\mathcal{F}\left(G^{\sigma}_{m,a,b}(R_{\theta,\phi}\boldsymbol{x})\right) = & \sum_{u_1=0}^{m-a}\sum_{v_1=0}^{a-b}\sum_{w_1=0}^{b}\sum_{u_2=0}^{u_1}\sum_{w_2=0}^{w_1}\psi^{(u_1,v_1,w_1,u_2,w_2)^{\mathrm{T}}}_{m,a,b}\cdot\hat{G}^{\sigma}(\boldsymbol{\omega}) \\ & (i\omega_x)^{m-(u_1+v_1+w_1)}(i\omega_y)^{(u_1+v_1+w_1)-(u_2+w_2)}(i\omega_z)^{u_2+w_2} \quad ,\end{aligned} \tag{6}$$

where

$$\begin{aligned}\psi^{(u_1,v_1,w_1,u_2,w_2)^{\mathrm{T}}}_{m,a,b} = & (-1)^{a-v_1-w_2}\binom{m-a}{u_1}\binom{a-b}{v_1}\binom{b}{w_1}\binom{u_1}{u_2}\binom{w_1}{w_2} \\ & (\cos\theta)^{m-a-u_2+w_2}(\cos\phi)^{m-a+b-u_1+v_1-w_1} \\ & (\sin\theta)^{b+u_2-w_2}(\sin\phi)^{a-b+u_1-v_1+w_1-u_2-w_2} \quad .\end{aligned} \tag{7}$$

Applying the inverse FT to Equation (6) and convolving with image I finally yields:

$$\begin{aligned}I * G^{\sigma}_{m,a,b}(R_{\theta,\phi}\boldsymbol{x}) &= \sum_{u_1,v_1,w_1,u_2,w_2}\psi^{(u_1,v_1,w_1,u_2,w_2)^{\mathrm{T}}}_{m,a,b}\left(I * G^{\sigma}_{m,u_1+v_1+w_1,u_2+w_2}\right)(\boldsymbol{x}) \\ &= \sum_{i=0}^{m}\sum_{j=0}^{i}\underbrace{\sum_{\boldsymbol{s}\in\mathcal{S}^{i,j}_{m,a,b}}\psi^{\boldsymbol{s}}_{m,a,b}}_{w^{i,j}_{m,a,b}}\underbrace{\left(I * G^{\sigma}_{m,i,j}\right)(\boldsymbol{x})}_{\boldsymbol{f_{m,i,j}}(I,\boldsymbol{x})} \quad ,\end{aligned} \tag{8}$$

where

$$\begin{aligned}\mathcal{S}^{i,j}_{m,a,b} = \{(u_1,v_1,w_1,u_2,w_2)^{\mathrm{T}} \in \mathbb{N}_0^5 \mid & u_1 \le m-a,\ v_1 \le a-b, \\ & w \le b,\ u_2 \le u_1,\ w_2 \le w_1, \\ & u_1+v_1+w_1 = i, u_2+w_2 = j\} \quad .\end{aligned} \tag{9}$$

□

A.2 Segmentation Results

The binary segmentation of the cerebrovascular networks of the test ROIs of datasets $\mathcal{D}_{1-4}$ are compared for the different vessel segmentation approaches in Figures 1-4.

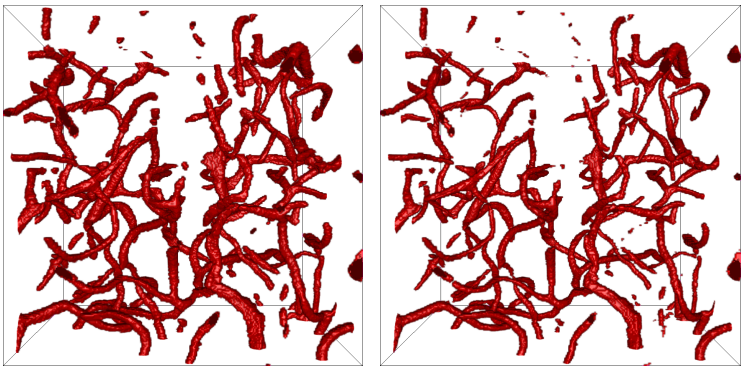

(a) Ground Truth **(b)** Otsu

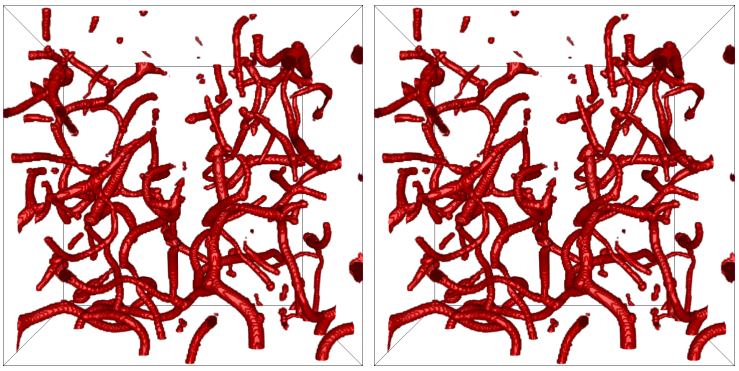

(c) Frangi **(d)** Sato

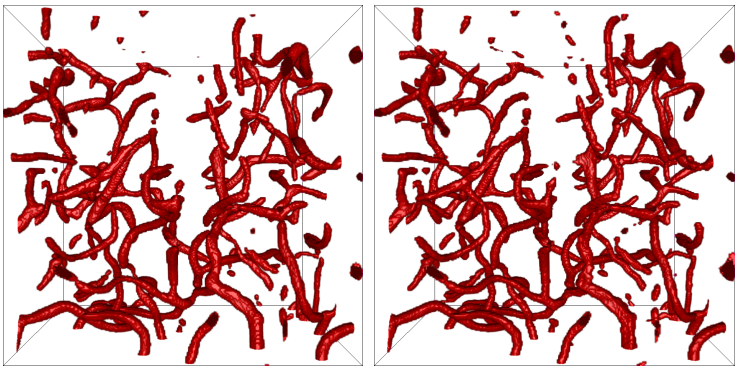

(e) RF-OSF **(f)** RF-SFT

Fig. 1: Segmented cerebrovascular network for whole 3-D test ROI of dataset $\mathcal{D}_1$ using different segmentation techniques. (a) Ground truth. (b) Otsu's method [4]. (c) Frangi [1]. (d) Sato [5]. (e) RF-OSF ($d = 102$). (f) RF-SFT ($M = 4$). The binary segmentation maps are computed at the corresponding F_1-optimal operating points.

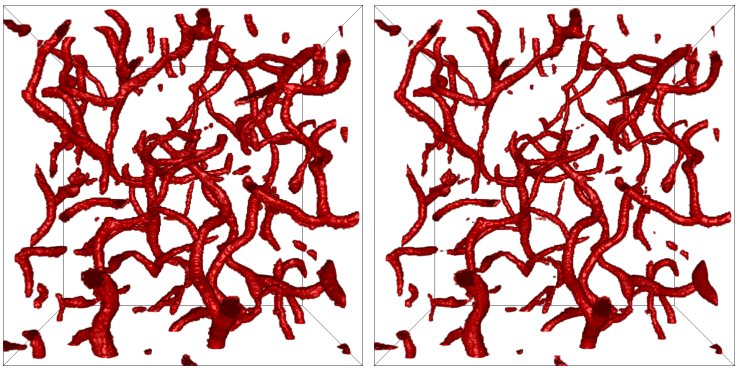

(a) Ground Truth **(b)** Otsu

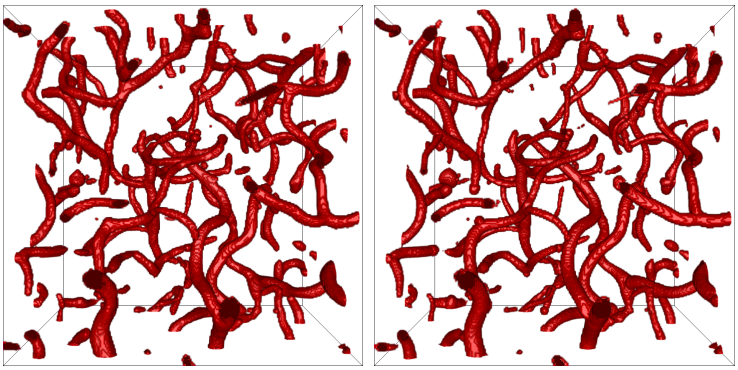

(c) Frangi **(d)** Sato

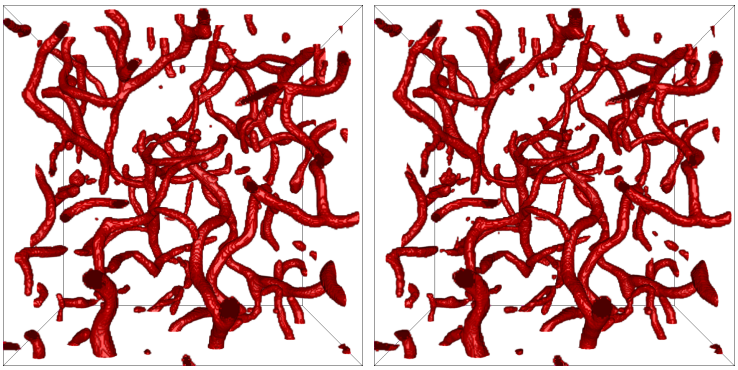

(e) RF-OSF **(f)** RF-SFT

Fig. 2: Segmented cerebrovascular network for whole 3-D test ROI of dataset $\mathcal{D}_2$ using different segmentation techniques. (a) Ground truth. (b) Otsu's method [4]. (c) Frangi [1]. (d) Sato [5]. (e) RF-OSF ($d = 102$). (f) RF-SFT ($M = 4$). The binary segmentation maps are computed at the corresponding F_1-optimal operating points.

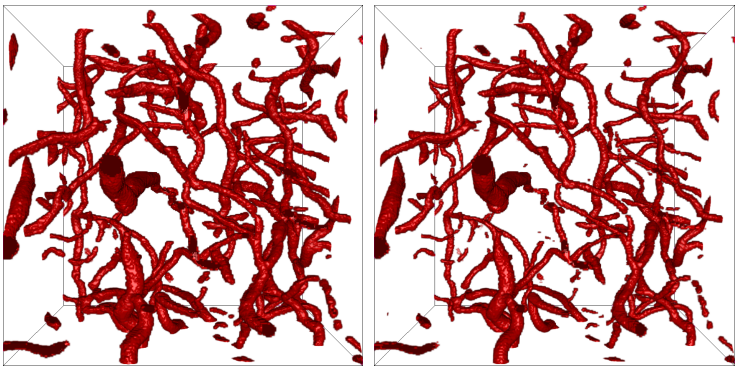

(a) Ground Truth

(b) Otsu

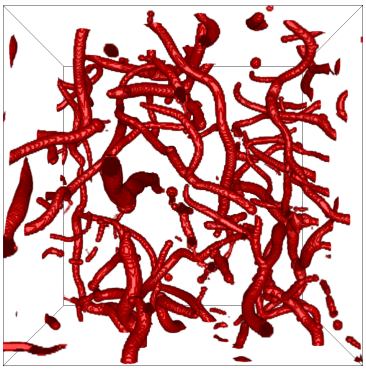

(c) Frangi

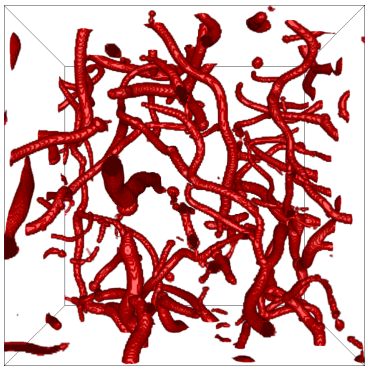

(d) Sato

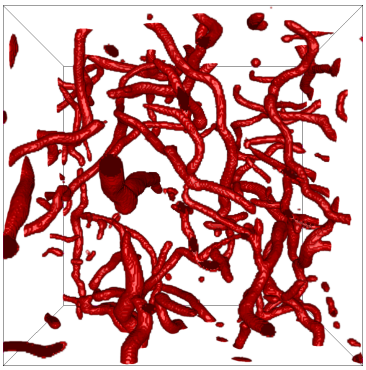

(e) RF-OSF

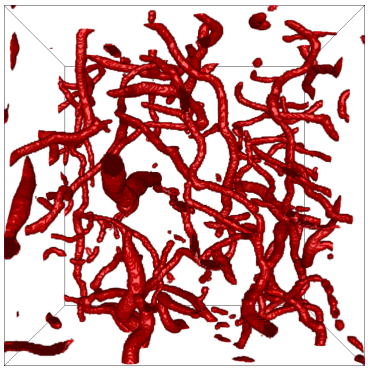

(f) RF-SFT

Fig. 3: Segmented cerebrovascular network for whole 3-D test ROI of dataset $\mathcal{D}_3$ using different segmentation techniques. (a) Ground truth. (b) Otsu's method [4]. (c) Frangi [1]. (d) Sato [5]. (e) RF-OSF ($d = 102$). (f) RF-SFT ($M = 4$). The binary segmentation maps are computed at the corresponding F_1-optimal operating points.

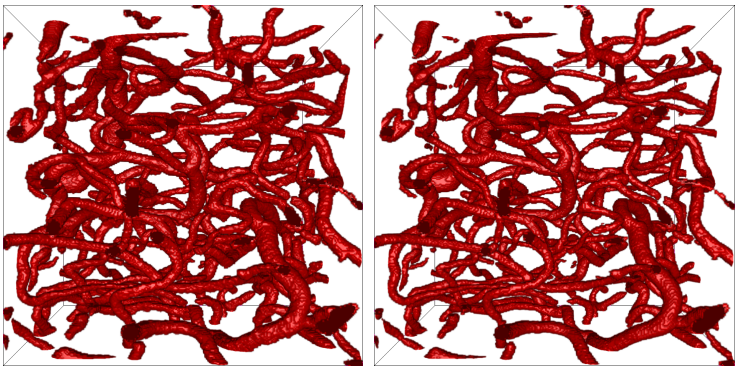

(a) Ground Truth **(b)** Otsu

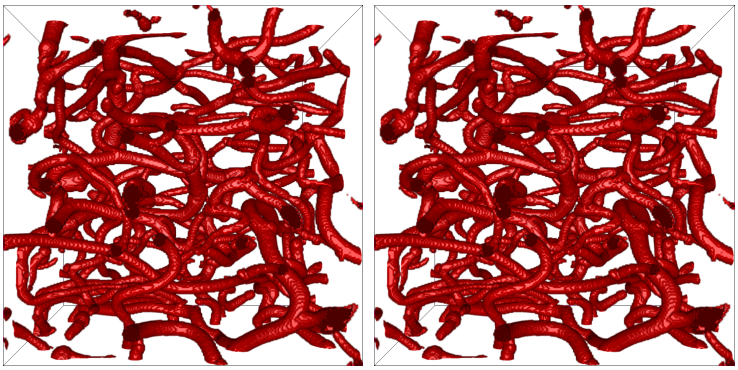

(c) Frangi **(d)** Sato

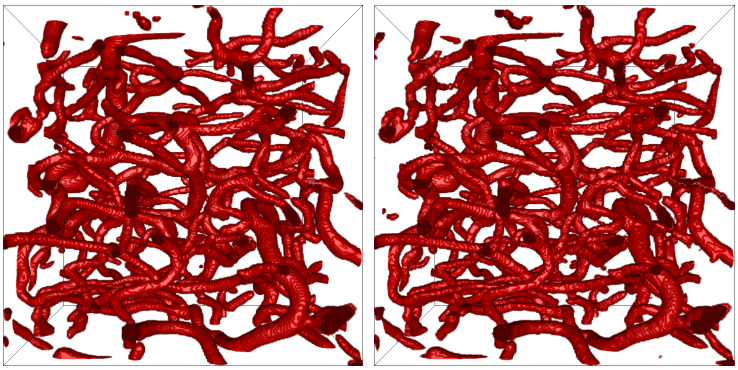

(e) RF-OSF **(f)** RF-SFT

Fig. 4: Segmented cerebrovascular network for whole 3-D test ROI of dataset $\mathcal{D}_4$ using different segmentation techniques. (a) Ground truth. (b) Otsu's method [4]. (c) Frangi [1]. (d) Sato [5]. (e) RF-OSF ($d = 102$). (f) RF-SFT ($M = 4$). The binary segmentation maps are computed at the corresponding F_1-optimal operating points.

References

1. Frangi, A., Niessen, W., Vincken, K., Viergever, M.: Multiscale vessel enhancement filtering. In: Wells, W., Colchester, A., Delp, S. (eds.) MICCAI'98. LNCS, vol. 1496, pp. 130–137. Springer, Berlin/Heidelberg (1998)
2. Freeman, W.T., Adelson, E.H.: The design and use of steerable filters. IEEE Trans Pattern Anal Mach Intell 13(9), 891–906 (Sep 1991)
3. Jacob, M., Unser, M.: Design of steerable filters for feature detection using canny-like criteria. IEEE Trans Pattern Anal Mach Intell 26(8), 1007–1019 (Aug 2004)
4. Otsu, N.: A threshold selection method from gray-level histograms. IEEE T Syst Man Cyb 9(1), 62–66 (Jan 1979)
5. Sato, Y., Nakajima, S., Atsumi, H., Koller, T., Gerig, G., Yoshida, S., Kikinis, R.: 3D multi-scale line filter for segmentation and visualization of curvilinear structures in medical images. In: Troccaz, J., Grimson, E., Mösges, R. (eds.) CVRMed-MRCAS'97. LNCS, vol. 1205, pp. 213–222. Springer Berlin / Heidelberg (1997)